

Multiscale spatial Monte Carlo simulations: Multigriding, computational singular perturbation, and hierarchical stochastic closures

Abhijit Chatterjee and Dionisios G. Vlachos^{a)}

*Department of Chemical Engineering, University of Delaware, Newark, Delaware 19716
and Center for Catalytic Science and Technology (CCST), University of Delaware,
Newark, Delaware 19716*

(Received 22 September 2005; accepted 13 December 2005; published online 14 February 2006)

Monte Carlo (MC) simulation of most spatially distributed systems is plagued by several problems, namely, execution of one process at a time, large separation of time scales of various processes, and large length scales. Recently, a coarse-grained Monte Carlo (CGMC) method was introduced that can capture large length scales at reasonable computational times. An inherent assumption in this CGMC method revolves around a mean-field closure invoked in each coarse cell that is inaccurate for short-ranged interactions. Two new approaches are explored to improve upon this closure. The first employs the local quasichemical approximation, which is applicable to first nearest-neighbor interactions. The second, termed multiscale CGMC method, employs singular perturbation ideas on multiple grids to capture the entire cluster probability distribution function via short microscopic MC simulations on small, fine-grid lattices by taking advantage of the time scale separation of multiple processes. Computational strategies for coupling the fast process at small length scales (fine grid) with the slow processes at large length scales (coarse grid) are discussed. Finally, the binomial τ -leap method is combined with the multiscale CGMC method to execute multiple processes over the entire lattice and provide additional computational acceleration. Numerical simulations demonstrate that in the presence of fast diffusion and slow adsorption and desorption processes the two new approaches provide more accurate solutions in comparison to the previously introduced CGMC method. © 2006 American Institute of Physics. [DOI: 10.1063/1.2166380]

I. INTRODUCTION

Over the last few years, emphasis has been placed on the development of lattice kinetic Monte Carlo (KMC) models for applications ranging from catalysis to separations to atmospheric sciences to epitaxial growth to biology.^{1–7} While these models provide significant insight into microscopic and mesoscopic scale phenomena, they cannot easily be extended to study large scales for several reasons. First, in KMC one at a time process is selected out of several possible ones. This approach limits KMC to systems with a few processes, to small populations for well-mixed systems, and to small lattices for spatially distributed systems. Second, in most physical systems there is a separation of time scales between physical processes. This aspect, known in computer science as stiffness, results in frequent sampling of fast processes and rare sampling of slow processes. For example, in most surface deposition experiments the ratio of the diffusion to adsorption fluxes is large (e.g., 10^5 or higher).⁸ Similar time scale issues arise in catalysis.⁹ Given that the time step is mainly controlled by the fast processes, the time advanced in stiff systems via a conventional KMC is too short.

Recent research efforts, reviewed in Ref. 10, aiming at acceleration of KMC have mainly focused on well-mixed systems.^{11–15} In parallel, we have been developing a multiscale stochastic mathematical and simulation framework,

called coarse-grained Monte Carlo (CGMC) method,^{16–18} for spatially distributed systems. The CGMC method uses a coarse grid to enable simulation of large length scales at a reasonable computational cost by effectively reducing the number of cells and processes and possibly by shortening the interaction potential. The challenge in any accelerated KMC method lies in accurately coarse graining the underlying microscopic physics. So far the local mean-field (MF) stochastic closure has been invoked in the CGMC method to arrive at an analytical expression for the transition probabilities as a function of coarse observables. This closure assumes that the probability distribution function (pdf) of particles (herein particle refers to atoms, molecules, or other species interacting on a lattice) within each coarse cell is uniform. The MF closure is too poor an approximation, especially when interactions between particles are short ranged.

In order to improve the accuracy of the CGMC method, in this paper a hierarchy of stochastic closures is explored ranging from the existing MF to the local quasichemical (QC) approximation¹⁹ to a new multiscale CGMC method. The latter method explicitly exploits the separation of time scales between various processes by a technique that is reminiscent of singular perturbation. Its construction allows one to compute the entire pdf on a fine grid over short time scales and pass this information to the coarse grid governed by slow processes and thus to retain the correct noise between scales at substantially lower computational cost. This feature is important when modeling phenomena where fluctuations

^{a)}Author to whom correspondence should be addressed. Fax: (302) 831-1048. Electronic mail: vlachos@che.udel.edu

and spatial correlations play an important role. In addition, the binomial τ -leap method of executing multiple processes per time increment¹⁴ is combined with the multiscale CGMC method to provide further time acceleration. It is demonstrated that the multiscale CGMC method gives statistically indistinguishable results from those of the KMC method.

The structure of this paper is as follows. The microscopic lattice model is briefly described in Sec. II. The CGMC method along with the results of singular perturbation method (see the Appendix) based on time scale separation of various processes are outlined in Sec. III. Various closures and the new multiscale CGMC method are discussed in Sec. IV. Detailed balance is addressed in Sec. V. Algorithms are outlined in Sec. VI, followed by numerical simulations in Sec. VII. Finally conclusions are provided in Sec. VIII.

II. MICROSCOPIC LATTICE MODEL

In the microscopic model, a lattice \mathcal{L} consists of N sites that denote potential minima where particles can reside. Each site $v \in \mathcal{L}$ is characterized by an occupancy function σ_v that takes a value of 1, when the site is occupied, or 0, when it is unoccupied. Let $\underline{\sigma}$ be the configuration-space vector containing the time-dependent occupation functions on \mathcal{L} . The Hamiltonian of the microscopic lattice is given by

$$H(\underline{\sigma}) = -\frac{1}{2} \sum_{v \in \mathcal{L}} \sum_{\substack{v' \in \mathcal{L} \\ v' \neq v}} J(|v - v'|) \sigma_v \sigma_{v'} + \sum_{v \in \mathcal{L}} h \sigma_v, \quad (1)$$

where h is an external field, such as the chemical potential. Here the two-body interaction potential $J(r)$ describes the strength of lateral particle-particle interactions, and $r = |v - v'|$ is the distance between sites v and v' . The convention followed in this paper is that $J(r)$ is positive (negative) for attractive (repulsive) interactions. The interaction energy U_v of an adsorbed particle at site v with the rest of the adsorbed particles on the lattice is

$$U_v(\underline{\sigma}) = \sum_{v' \in \mathcal{L}, v' \neq v} J(|v - v'|) \sigma_{v'}. \quad (2)$$

The maximum dimensionless interaction of a particle at a site occurs when all sites are occupied.

$$\beta J_0 = \beta \sum_{\substack{v, v' \in \mathcal{L} \\ 1 \leq |v - v'| \leq L_p}} J(|v - v'|), \quad (3)$$

where $\beta = (k_B T)^{-1}$, k_B is the Boltzmann constant, T is the absolute temperature, and L_p is the interaction potential length. For nearest-neighbor (NN) interactions ($L_p = 1$) of strength $J_{\text{NN}} = J_0/c$, which are considered in the numerical examples of this paper, the Hamiltonian is given by

$$H(\underline{\sigma}) = -\frac{1}{2} J_{\text{NN}} \sum_{j=0}^c n_j + \sum_{v \in \mathcal{L}} h \sigma_v. \quad (4)$$

Here c is the coordination number of the lattice [e.g., $c=4$ for the (100) square lattice] and n_j is the number of occupied

TABLE I. Transition probability per unit time of microscopic processes. The prefactors for adsorption and desorption are those of the corresponding mean-field model. Γ_m is the 2D diffusion hopping frequency when the coordination number is $c=4$; the factor of $1/4$ appears since there is an equal probability of an adsorbed particle hopping in any of the four directions.

Process	Transition probability per unit time
Adsorption	$\Gamma_a(v) = \begin{cases} k_a P = d_0, & \sigma_v = 0 \\ 0, & \sigma_v = 1, \end{cases}$ or equivalently $\Gamma_a(v) = k_a P(1 - \sigma_v)$
Desorption	$\Gamma_d(v) = \begin{cases} 0, & \sigma_v = 0 \\ k_d e^{-\beta U_v} = d_0 e^{\beta(h - U_v)}, & \sigma_v = 1, \end{cases}$ or equivalently $\Gamma_d(v) = k_d \sigma_v e^{-\beta U_v}$
Diffusion	$\Gamma_{\text{mig}}(v \rightarrow v') = \begin{cases} 0, & \sigma_v = 0 \\ \Gamma_m e^{-\beta U_v/4}, & \sigma_v = 1, \sigma_{v'} = 0 \\ 0, & \sigma_v = 1, \sigma_{v'} = 1, \end{cases}$ or equivalently $\Gamma_{\text{mig}}(v \rightarrow v') = \frac{\Gamma_m}{4} \sigma_v (1 - \sigma_{v'}) e^{-\beta U_v}$

sites on the lattice with j occupied NNs, $j = \{0, 1, \dots, c\}$.

The starting point for a stochastic description of the system is the master equation²⁰

$$\frac{dP(\underline{\sigma})}{dt} = \sum_{\substack{\underline{\sigma}' \\ \underline{\sigma}' \neq \underline{\sigma}}} G(\underline{\sigma}' \rightarrow \underline{\sigma}) P(\underline{\sigma}') - \sum_{\substack{\underline{\sigma}' \\ \underline{\sigma}' \neq \underline{\sigma}}} G(\underline{\sigma} \rightarrow \underline{\sigma}') P(\underline{\sigma}) \quad (5)$$

that gives the probability $P(\underline{\sigma})$ of observing state $\underline{\sigma}$. $G(\underline{\sigma} \rightarrow \underline{\sigma}')$ is the transition probability per unit time of transition from state $\underline{\sigma}$ to state $\underline{\sigma}'$. Alternatively, one can write a difference-differential equation²¹

$$d\sigma_v = \sum_p \Gamma_p^+(v, \underline{\sigma}) dt - \sum_p \Gamma_p^-(v, \underline{\sigma}) dt \quad (6)$$

that gives the temporal evolution of the occupancy function at site v in terms of the transition probability per unit time $\Gamma_p^+(v, \underline{\sigma})$ [$\Gamma_p^-(v, \underline{\sigma})$] of process p that leads to a particle addition (deletion) at site v .

In this paper, a simple prototype system is studied for demonstrating the various multiscale coarse graining ideas introduced. However, our approach is sufficiently general and can be used for more complex systems. Three microscopic processes are considered. These include adsorption of a particle from the adjacent fluid phase to an empty-lattice site, desorption of an adsorbed particle from an occupied site to the fluid phase, and diffusion, i.e., an adsorbed particle hopping to a nearest-neighboring empty-lattice site. The transition probabilities per unit time Γ_p for these processes are typically postulated and are tabulated in Table I. In Table I and below we use the simplified notations $\Gamma_a(v)$ and $\Gamma_d(v)$ for the transition probabilities per unit time of adsorption and desorption at site v , respectively, and $\Gamma_{\text{mig}}(v \rightarrow v')$ for transition probabilities per unit time of a hop from site v to v' , despite the desorption and migration probabilities being dependent on $\underline{\sigma}$ via the interaction energy $U_v(\underline{\sigma})$.

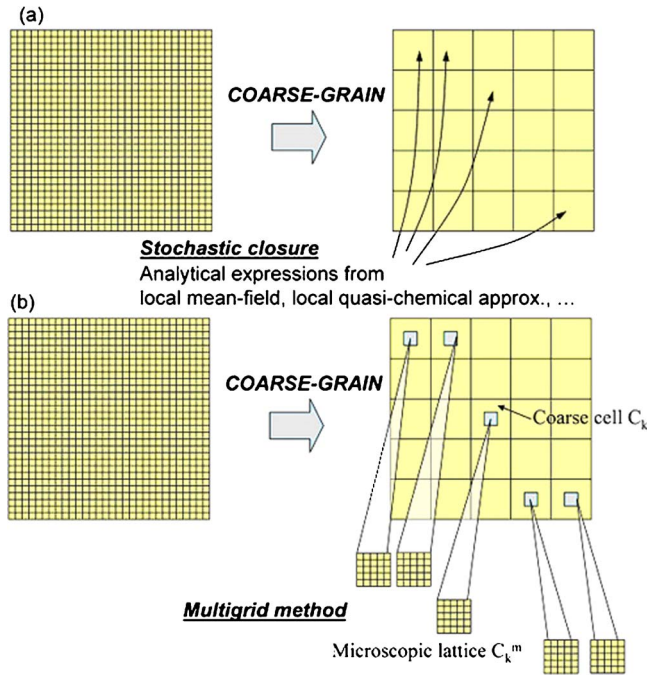


FIG. 1. (Color online) Schematic of different approaches for passing microscopic scale information to the coarse scale. (a) Enforcing stochastic closure via approximations for various moments of the cluster probability distribution function (pdf). (b) Estimating the cluster pdf using multiple grids.

The effect of interactions between adsorbed particles on the activation energy is accounted for using Arrhenius dynamics.^{22,23} Specifically, the activation energy of hopping is taken to depend only on the departing site given by Eq. (2). The activation energy of an adsorbed particle on an empty substrate (i.e., in the absence of lateral interactions), denoted as U_0 , is lumped into the prefactors k_d and Γ_m (see Table I). The lattice processes are assumed to be Markov processes. Equation (6) is solved numerically using the KMC method.

III. THE COARSE-GRAINED MONTE CARLO (CGMC) METHOD

A. Coarse lattice variables, transition probabilities, and energetics

We outline the CGMC method in this section. Details can be found in Refs. 16–18. The first step in CGMC is to group q microscopic sites of \mathcal{L} into coarse cells C_k to form a coarse lattice \mathcal{L}_c (see Fig. 1). Here q is an integer that determines the level of coarse graining. Site conservation requires that \mathcal{L}_c consists of $m=N/q$ uniformly sized coarse cells, where m is also an integer. One defines $\eta_k = \sum_{v \in C_k} \sigma_v$ as the coarse-grained occupancy in the k th cell C_k , i.e., the number of particles in C_k , where $0 \leq \eta_k \leq q$ and $1 \leq k \leq m$, and η as the vector of time-dependent coarse-grained occupancies of all cells. This vector is the main observable of a CGMC simulation. We define the cell coverage, i.e., the fraction of occupied sites of C_k , as $\bar{\eta}_k = \eta_k/q$ and the spatially averaged coverage over the entire lattice as $\theta = \sum_{k=1}^m \bar{\eta}_k/m$.

Assuming k_d and $k_a P$ to be constant, the coarse-grained transition probability per unit time for adsorption can easily

TABLE II. Coarse-grained transition probability per unit time of slow processes used in the CGMC methods (assuming large coarse-cell size, i.e., $q \rightarrow \infty$).

Process	Transition probability per unit time
Adsorption	$\bar{\Gamma}_a(k) = k_a P(q - \eta_k)$
Desorption	$\bar{\Gamma}_d(k) = k_d \sum_{v \in C_k} \langle \sigma_v e^{-\beta U_v} \rangle$

be expressed in terms of the coarse variable η_k as follows (overbars are hereafter used to denote the corresponding coarse-grained variables):

$$\begin{aligned} \bar{\Gamma}_a(k) &= \left\langle \sum_{v \in C_k} \Gamma_a(v) \right\rangle = \sum_{v \in C_k} k_a P(1 - \langle \sigma_v \rangle) \\ &= k_a P(q - \eta_k), \quad k = 1, \dots, m. \end{aligned} \quad (7)$$

In the case of desorption, the coarse-grained transition probability per unit time is

$$\bar{\Gamma}_d(k) = \left\langle \sum_{v \in C_k} \Gamma_d(v) \right\rangle = \sum_{v \in C_k} k_d \langle \sigma_v e^{-\beta U_v} \rangle, \quad k = 1, \dots, m. \quad (8)$$

These results are summarized in Table II. The difficulty here is that spatial correlations on the microscopic lattice make the connection between the average of the last term and the coarse variable η_k difficult. The same is true for diffusion between coarse cells. Likewise, spatial correlations determine the coarse Hamiltonian

$$\bar{H}(\underline{\sigma}) = \sum_{k \in \mathcal{L}} \bar{H}_1(k) + \bar{H}_2(k) + \bar{H}_{\text{ext}}(k). \quad (9)$$

Here, the contribution from interactions between C_k and other cells C_j is given by

$$\bar{H}_1(k) = -\frac{1}{2} \sum_{v \in C_k} \sum_{\substack{v' \in C_j \\ j \neq k}} \langle J(|v - v'|) \sigma_v \sigma_{v'} \rangle, \quad (10)$$

and the contribution from interactions within C_k is given by

$$\bar{H}_2(k) = -\frac{1}{2} \sum_{v \in C_k} \sum_{\substack{v' \in C_k \\ v' \neq v}} \langle J(|v - v'|) \sigma_v \sigma_{v'} \rangle. \quad (11)$$

$\bar{H}_{\text{ext}}(k) = \bar{h} \eta_k$ gives the contribution of the coarse external field \bar{h} . Again, the challenge is how to connect these coarse quantities (transition probabilities and energetics) with the coarse observable $\underline{\eta}$. In order to achieve this task, some closure is necessary.

B. Separation of time scales and local equilibrium

In our previous work, it was tacitly assumed that local equilibrium exists within each coarse cell. This local equilib-

rium implies a separation of time scales, namely, some processes relax much faster than the rest. Here we explicitly exploit this separation of time scales in order to put a firm foundation to the multiscale CGMC method discussed later. For our specific model system, the separation of time scales is achieved via taking diffusion to be fast compared to adsorption and desorption ($\Gamma_m \gg k_a P, k_d$), a very common physical situation. In other systems, other choices may be more suitable. It is shown in the Appendix that the configuration space evolves at fast time scales $\tilde{t}_f = \Gamma_m t$ according to

$$d \sum_{v \in C_k} \langle \sigma_v(\tilde{t}_f) \rangle = \frac{1}{4} d\tilde{t}_f \sum_{v \in C_k} \sum_{v' \in B_v} (\langle \sigma_{v'}(1 - \sigma_v) e^{-\beta U_{vv'}} \rangle - \langle \sigma_v(1 - \sigma_{v'}) e^{-\beta U_{vv'}} \rangle), \quad (12)$$

whereas the slow processes of adsorption and desorption and the coarse occupation variables remain fixed at short times. Here B_v is the set of sites around v to (from) which diffusion from (to) site v can occur (see also the Appendix). Since diffusion is fast, the coarse cell is *locally equilibrated* in a short time (relaxation time) determined by Γ_m , after which Eq. (12) gives

$$\sum_{v \in C_k} \sum_{v' \in B_v} (\langle \sigma_{v'}(1 - \sigma_v) e^{-\beta U_{vv'}} \rangle - \langle \sigma_v(1 - \sigma_{v'}) e^{-\beta U_{vv'}} \rangle) = 0. \quad (13)$$

The configuration space evolves over the slow time scales $\tilde{t}_s = k_a P t$ of interest according to

$$d \sum_{v \in C_k} \langle \sigma_v(\tilde{t}_s) \rangle = d\tilde{t}_s \sum_{v \in C_k} (1 - \langle \sigma_v \rangle) - \omega \langle \sigma_v e^{-\beta U_v} \rangle \quad (14)$$

subject to Eq. (13) (see the Appendix). Here $\omega = k_d/k_a P$. This approach is reminiscent of adiabatic elimination in stochastic differential equations.^{20,24} Equation (14) is projected to the coarse lattice and the corresponding coarse-grained difference-differential equation is given by

$$d\eta_k = \bar{\Gamma}_d(k) dt - \bar{\Gamma}_d(k) dt. \quad (15)$$

In passing we should note that the separation of time scales results in decoupling of fast processes [studied at short times in the canonical (NVT) ensemble in this case] and slow processes [studied at long times in the grand canonical (μVT) ensemble in this case]. Such decoupling arises for all models that exhibit (in continuum nomenclature) a spectral gap, i.e., which they have a large separation of time scales, but may not necessarily result in simulations done in different ensembles. Reference 25 provides an example of fast and slow chemical reactions, without any diffusion, where no decoupling of ensembles happens. Many physical systems exhibit such a large separation of time scales. In our case, the time-dependent coarse variables, such as the coarse coverage obtained from applying Eq. (15), are constraints in Eq. (13). In turn, the underlying pdf of microscopic states, given by Eq. (13), dictates the transition probabilities of slow processes firing according to Eq. (15). Even though an analytical expression for the exact equilibrium pdf with NN interactions is known for the one-dimensional (1D) lattice,¹⁹ so far the exact two-dimensional (2D) and three-dimensional (3D)

lattice pdfs are not available for the general case. When the exact equilibrium pdf is not available, a stochastic closure is employed to eliminate Eq. (13) and approximate spatial correlations along with their effect on the coarse transition probabilities [Fig. 1(a)]. Alternatively, one may employ multiple grids to numerically solve both Eqs. (13) [or its time-dependent version Eq. (12) and (15) [Fig. 1(b)]. These approaches are discussed in the next section.

IV. STOCHASTIC CLOSURES

A. Local mean-field (MF) approximation

In the local MF approximation, one assumes a random distribution of particles and disregards any local correlations between particles inside a coarse cell. The coarse-grained Hamiltonian on \mathcal{L}_c was derived previously in Refs. 16 and 17 as [compare to Eq. (9)]

$$\bar{H}(\underline{\eta}) = -\frac{1}{2} \left[\sum_{k \in \mathcal{L}_c} \sum_{\substack{j \in \mathcal{L}_c \\ j \neq k}} \bar{J}_{kj} \eta_k \eta_j + \sum_{k \in \mathcal{L}_c} \bar{J}_{kk} \eta_k (\eta_k - 1) \right] + \sum_{k \in \mathcal{L}_c} \bar{H}_{\text{ext}}(k) h \eta_k. \quad (16)$$

\bar{J}_{kk} is the coarse-grained potential within cell C_k and \bar{J}_{kj} is the coarse-grained potential between cells C_k and C_j .^{16,17} The coarse-grained potentials are real-valued constants evaluated in the beginning of a CGMC simulation using wavelets.

In order to obtain dynamics, a systematic procedure for coarse graining the microscopic transition probabilities per unit time of various processes was introduced in Ref. 26. The coarse-grained interaction energy between adsorbed sites using the local MF approximation is given by

$$\bar{U}_k = \bar{J}_{kk}(\eta_k - 1) + \sum_{l \in \mathcal{L}_c, l \neq k} \bar{J}_{kl} \eta_l. \quad (17)$$

Neglecting the spatial correlations in Eq. (8) one gets

$$\bar{\Gamma}_d(k) = \sum_{v \in C_k} k_d \langle \sigma_v e^{-\beta U_v} \rangle \approx k_d \eta_k e^{-\beta \bar{U}_k}. \quad (18)$$

Note that by using MF closure we are able to connect $\bar{\Gamma}_d(k)$ and \bar{U}_k with the coarse variable η_k . Hereafter, the CGMC method with the local MF closure is denoted as the CGMC-MF method.

It has been found through simulation and large deviation theory that the CGMC-MF method preserves the noise, does not suffer from numerical instabilities, and gives significant computational savings over KMC (see Refs. 16 and 17 for details). In the limit of infinitely long-ranged interactions and/or weak interactions and/or high temperatures, the local MF assumption is accurate. When this is not true, the local MF assumption results in information loss of the particle locations and correlations. For example, with short-ranged interactions many moments of the pdf are needed to describe the cluster size distribution, and the local MF assumption is a poor approximation. When the temperature is greater than the critical temperature, so that no phase separation is evi-

denced, the error of CGMC-MF is a function of the coarse-cell size, the strength and range of interactions, the occupancy, and the dimensionality of the lattice.²⁷

B. Local quasichemical (QC) approximation for nearest-neighbor (NN) interactions

Here the QC approximation (or the equivalent Bethe-Peierls approximation) is employed within each cell (termed as *local* QC theory) when NN interactions are present. In the local QC approximation, one works with four possible states of a pair of sites inside a coarse cell C_k , namely, both sites being occupied, one site out of the pair being occupied and both sites being unoccupied. All pairs are assumed to be independent of each other. The partition function for a large coarse cell C_k is written as

$$Q(\eta_k, q, T) = Q_s^{\eta_k} \sum_{N_{01}} g_{NN}(\eta_k, q, N_{01}^{NN}) \exp(\beta J_{NN} N_{11}^{NN}), \quad (19)$$

where the combinatorial factor $g_{NN}(\eta_k, q, N_{01}^{NN})$ gives the possible number of ways η_k occupied sites and $q - \eta_k$ vacant sites can be distributed among q sites, $Q_s = e^{-\beta h}$ is the partition function of a single adsorbed particle on the lattice, $N_{01}^{NN}(N_{11}^{NN})$ is the number of pairs with one site (both sites) occupied, and J_{NN} is the isotropic NN interaction potential between two neighboring adsorbed particles. The cell size q is assumed to be large enough to neglect boundary effects. Using the maximum term method, the partition function for the coarse cell C_k is¹⁹

$$Q(q, \eta_k, T) = Q_s^{\eta_k} Q_{NN}, \quad (20)$$

where

$$\sum_{v \in C_k} \langle \sigma_v e^{-\beta U_v} \rangle \approx \begin{cases} 0, & \bar{\eta}_k = 0 \\ \eta_k \left[\frac{(\zeta_{NN} - 1 + 2\bar{\eta}_k)(1 - \bar{\eta}_k)}{(\zeta_{NN} + 1 - 2\bar{\eta}_k)\bar{\eta}_k} \right]^{c/2} e^{-\beta J_{NN} c/2}, & 0 < \bar{\eta}_k < 1 \\ q e^{-\beta J_{NN} c}, & \bar{\eta}_k = 1. \end{cases} \quad (26)$$

Equation (26) is used in Eq. (8) and the coarse-grained transition probability per unit time for desorption is given by

$$\bar{\Gamma}_d(k) = \left\langle \sum_{v \in C_k} \Gamma_d(v) \right\rangle \approx \begin{cases} 0, & \bar{\eta}_k = 0 \\ k_d \eta_k \left[\frac{(\zeta_{NN} - 1 + 2\bar{\eta}_k)(1 - \bar{\eta}_k)}{(\zeta_{NN} + 1 - 2\bar{\eta}_k)\bar{\eta}_k} \right]^{c/2} e^{-\beta J_{NN} c/2}, & 0 < \bar{\eta}_k < 1 \\ k_d q e^{-\beta J_{NN} c}, & \bar{\eta}_k = 1. \end{cases} \quad (27)$$

Hereafter, the CGMC method with the local QC approximation will be denoted as the CGMC-QC method. Equations (25) and (27) are improvements over Eqs. (16) and (18) and are the key results of the CGMC-QC method. Like the local MF approximation, the local QC approximation provides an analytical expression connecting the transition probability

$$Q_{NN} = \left[\frac{q!}{\eta_k! (q - \eta_k)!} \right]^{1-c} \times \frac{(cq/2)!}{(c\eta_k/2 - N_{01}^{NN}/2)! (N_{01}/2)!^2 (c(q - \eta_k)/2 - N_{01}^{NN}/2)!} \quad (21)$$

is the configurational contribution to the partition function Q and $c=4$ is the coordination number of a 2D square lattice.

The adsorption isotherm is obtained by equating the chemical potential of the *coarse cell* C_k obtained from the QC approximation using Eq. (20) with the chemical potential of the fluid phase and is given by¹⁹

$$\lambda Q_s (1 - \bar{\eta}_k) = \bar{\eta}_k \left[\frac{(\zeta_{NN} - 1 + 2\bar{\eta}_k)(1 - \bar{\eta}_k)}{(\zeta_{NN} + 1 - 2\bar{\eta}_k)\bar{\eta}_k} \right]^{c/2} e^{-\beta J_{NN} c/2}, \quad (22)$$

where $\lambda = e^{\beta \mu}$, $0 < \bar{\eta}_k < 1$, and

$$\zeta_{NN} = \sqrt{1 - 4\bar{\eta}_k(1 - \bar{\eta}_k)(1 - e^{\beta J_{NN}})}. \quad (23)$$

The (configurational) energy of the cell is given by¹⁹

$$\bar{H}_2(k) = -\frac{cqJ_{NN}}{2} \left[\bar{\eta}_k - \frac{2\bar{\eta}_k(1 - \bar{\eta}_k)}{\zeta_{NN} + 1} \right]. \quad (24)$$

Neglecting boundary effects ($q \rightarrow \infty$), $\bar{H}_1(k) = 0$. Using Eq. (24), the Hamiltonian is given by [compare with Eq. (9)]

$$\bar{H}(\underline{\eta}) = \sum_{k \in \mathcal{L}_c} \bar{H}_2(k) + \sum_{k \in \mathcal{L}_c} \bar{h} \eta_k = - \sum_{k \in \mathcal{L}_c} \frac{cqJ_{NN}}{2} \times \left[\bar{\eta}_k - \frac{2\bar{\eta}_k(1 - \bar{\eta}_k)}{\zeta_{NN} + 1} \right] + \sum_{k \in \mathcal{L}_c} \bar{h} \eta_k. \quad (25)$$

Note that the right-hand side (rhs) of Eq. (22) provides the ensemble average

per unit time and energetics with computed observables of a CGMC simulation.

C. The multiscale CGMC method

An advantage of the aforementioned closures is that they analytically link the coarse energetics and transition prob-

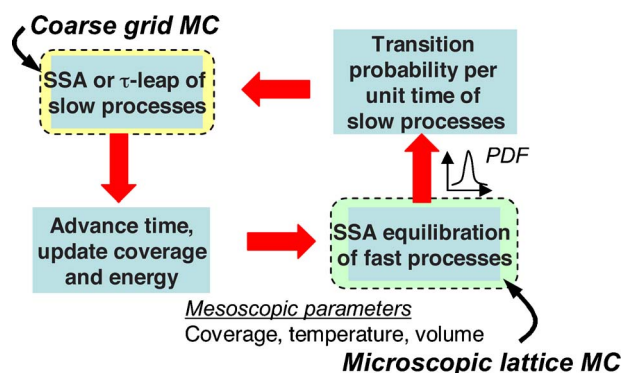


FIG. 2. (Color online) Schematic of the multiscale CGMC method. The algorithm consists of two integrators, namely, the coarse-grained lattice dynamics on slow processes/long times and the fast microscopic lattice equilibration on a small, fine grid for short times. Both integrators communicate with each other and exchange different length and time scales information.

abilities with the coarse observable η_k . However, the CGMC-MF is exact only when the potential is infinitely long (and in limiting cases where the temperature is infinitely high or the interaction is zero) and the CGMC-QC is a good approximation (but not exact) when the potential entails NN interactions only. More sophisticated approximations, such as cluster expansions, etc.,^{19,28} can also be employed to improve the accuracy but the accuracy usually improves slowly with increasing the number of moments of the pdf in comparison to the mathematical complexity needed.

There is obviously a need for a numerical method that is accurate for short-ranged potentials and is relatively easy to implement. This new approach is accomplished with a two-grid scheme. In the new method, a coarse grid of cell size q is employed to numerically solve Eq. (15) over large length scales, as in a regular CGMC simulation, but a small microscopic lattice of size q_m is also embedded within each coarse cell [see schematic in Fig. 1(b)] to solve Eq. (12). The overall idea, depicted in Fig. 2, is that the coarse variable η_k is used as a constraint while performing a KMC simulation of the fast processes on the fine grid within cell C_k . In turn, the fine-grid KMC simulations provide the correct pdfs needed for computing the transition probabilities of slow processes of a CGMC simulation on the coarse grid over long times.

Next we discuss time acceleration issues, some general issues of sampling states and processes when coupling simulations between scales followed by the equations for a specific example. Comparison of this new method to related work follows. Finally, the multiscale CGMC method is elaborated more in the algorithmic Sec. VI.

1. Time acceleration of the multiscale CGMC method

Significant acceleration can result when the size of the embedded fine-grid lattice q_m is much smaller than that of a coarse cell, i.e., $q_m \ll q$, because one computes the correct pdf by simulating, via the microscopic KMC method, only a small fraction q_m/q of the entire domain. This fact stems from the CPU that typically scales more than linearly with system size. Further acceleration results from the time scale separation, discussed in Sec. III B, between simulations on the two grids. Specifically, the microscopic KMC on the fine

grid needs only to be performed for short periods of time, of order $O(\Gamma_m^{-1})$, in comparison to the large time increments of the slow processes that are of order $O[(k_a P)^{-1}]$. As a result, one is able to evolve the system over macroscopic (or slow) time scales with the correct transition probabilities obtained from the underlying pdfs via short KMC simulations on small length, fine grids. These CPU savings are ideally of order $O(1/\varepsilon)$, where ε denotes the separation of time scales between diffusion and adsorption/desorption in our physical system (see also Appendix for its precise definition) but in reality are reduced due to the cost associated with the fast equilibration on the fine grid. It is clear that the larger the time separation is the faster the multiscale method will be. Further acceleration can result by maintaining the same pdf for a while and by firing multiple processes at once. These approaches are optional but we use them for the calculations of this paper and we discuss them in Sec. VI.

2. Computing pdfs and sampling of states on the fine grid

In the multigrid scheme, KMC simulations are performed on the microscopic lattice to obtain the probability $P_k^f(\sigma_k)$ of observing a configuration σ_k out of several equilibrium configurations $\{\sigma_k\}$. The subscript k denotes that the microscopic lattice is subject to the constraints imposed by coarse variables of C_k such as density, energy, temperature, pressure, etc. (in our case $\bar{\eta}_k, q_m, T$). The superscript f denotes that the pdf is obtained by running fast processes only. Typically the coarse cell and the microscopic lattice have different dimensions ($q_m \ll q$). Thus, $P_k^f(\sigma_k)$ encountered in the master Eq. (5) on a small fine lattice cannot directly be used on the coarse grid in solving Eq. (15) due to size (length scale) mismatch. Therefore, one needs to construct a pdf $\tilde{P}_k^f(x)$ of *relevant* states x that are common to both the microscopic and the coarse grids. We prefer to compute a pdf that is related to cluster size distribution and/or energy distribution. This choice stems from the fact that the transition probabilities of the slow processes depend precisely on such pdfs. For example, the form $\tilde{P}_k^f(x) \equiv P_j$ (the probability of an occupied site on the microscopic lattice with j occupied NNs) is used below.

One important point is how does one choose a microscopic state to fire from. An obvious method is to compute the time-average transition probabilities of the coarse processes (this is very easy to do during the microscopic KMC simulation) and then fire from an “average” microscopic state, the previous time step one, a random one, or even the last one. All of these could lead to pitfalls. The method of state and process selection has been detailed for well-mixed systems with disparity in time scales in Ref. 25. An important trait of our method is that while we compute the pdf of microscopic states on the fine grid, we do not have to compute an average microscopic state from which the evolution of slow processes occurs. Instead, the slow variables evolve from a microscopic state according to suitable probabilities. It is expected that firing from a microscopic state rather than an average state will be important for bistable and oscillating systems. One such numerical example is presented below but

these issues should be further explored in future work. Extending our work from Ref. 25, it turns out that the transition probability per unit time of firing the slow process p' from state x' in the coarse cell $C_{k'}$ is given by an average of the coarse cell

$$\bar{\Gamma}_{p'}^s(k', \underline{x}') = \sum_{v \in C_{k'}} \tilde{P}_{k'}^f(\underline{x}') \Gamma_{p'}^s(k', v, \underline{x}'), \quad (28)$$

where $\tilde{P}_{k'}^f(\underline{x}')$ is the probability of observing state \underline{x}' via the fast processes and $\Gamma_{p'}^s(k', v, \underline{x}')$ is the transition probability per unit time of firing out process p' from state \underline{x}' at site v of cell $C_{k'}$ (here the more explicit and general notation of transition probabilities is used). As a result, a slow process p' from a particular microscopic state \underline{x}' in cell $C_{k'}$ is selected with a probability (from a uniform distribution)

$$\frac{\sum_{v \in C_{k'}} \tilde{P}_{k'}^f(\underline{x}') \Gamma_{p'}^s(k', v, \underline{x}')}{\sum_{k \in \mathcal{L}_c} \sum_{\underline{x}} \sum_p \sum_{v \in C_k} \tilde{P}_k^f(\underline{x}) \Gamma_p^s(k, v, \underline{x})}. \quad (29)$$

In the denominator we sum over all slow processes p and over the entire lattice as happens in any microscopic KMC. The lack of overbars on the rhs of Eqs. (28) and (29) indicates that the transition probabilities of slow processes are microscopic and are computed from the pdf of the fast processes. Using Eq. (28), Eq. (29) becomes

$$\frac{\bar{\Gamma}_{p'}^s(k', \underline{x}')}{\sum_{k \in \mathcal{L}_c} \sum_{\underline{x}} \sum_p \bar{\Gamma}_p^s(k, \underline{x})}. \quad (30)$$

Since the slow variables do not change by the fast variables (canonical ensemble fine-grid simulations) in our model system, in the simulations that follow the stochastic average transition probability per unit time is computed by summing over all microscopic states of each coarse cell. The transition probability per unit time of firing a slow process p' from all possible states in cell $C_{k'}$ is

$$\bar{\Gamma}_{p'}^s(k') = \sum_{\underline{x}} \sum_{v \in C_{k'}} \tilde{P}_{k'}^f(\underline{x}) \Gamma_{p'}^s(k', v, \underline{x}). \quad (31)$$

The probability of firing the slow process p' among all processes over the entire coarse lattice is then

$$\frac{\sum_{\underline{x}} \sum_{v \in C_{k'}} \tilde{P}_{k'}^f(\underline{x}) \Gamma_{p'}^s(k', v, \underline{x})}{\sum_{k \in \mathcal{L}_c} \sum_{\underline{x}} \sum_p \sum_{v \in C_k} \tilde{P}_k^f(\underline{x}) \Gamma_p^s(k, v, \underline{x})} = \frac{\bar{\Gamma}_{p'}^s(k')}{\sum_{k \in \mathcal{L}_c} \sum_p \bar{\Gamma}_p^s(k)}. \quad (32)$$

Alternatively, by computing the probability of observing a state from its average lifetime,²⁹ one has a simple way to evaluate the transition probabilities of slow processes on the fly of the microscopic KMC on the fine grid [instead of using Eq. (31)]

$$\bar{\Gamma}_{p'}^s(k') = \frac{q}{q_m} \sum_i \sum_{v \in C_{k'}^m} \Delta t_{k',m}^i \Gamma_{p'}^s(k', v) \Big/ \sum_i \Delta t_{k',m}^i, \quad (33)$$

where $\Delta t_{k',m}^i$ is the i th time increment of the microscopic KMC event on the fine grid and $t_m = \sum_i \Delta t_{k',m}^i$ is the total (relatively short) time simulated by the KMC on the microscopic grid lattice $C_{k'}^m$ in the coarse cell $C_{k'}$ [see Fig. 1(b)] at equilibrium (after an initial, discarded period needed to compute equilibrium statistics).

3. An example of computing the pdf and coarse transition probabilities on the fine grid

Next we derive the $\tilde{P}_k^f(\underline{x})$ for the system studied in this paper. The coarse-grained adsorption transition probability per unit time given by Eq. (7) is a linear function of the coarse variable and, as such, it does not contain any spatial correlations, i.e., it is exact. The desorption transition probability per unit time is given by

$$\begin{aligned} \bar{\Gamma}_d(k) &= k_d \left\langle \sum_{v \in C_k} \sigma_v \exp(-\beta U_v) \right\rangle \\ &= k_d \left\langle \sum_{v \in C_k}^* \exp(-\beta U_v) \right\rangle. \end{aligned} \quad (34)$$

Here the asterisk indicates summation over all occupied sites within cell C_k (where $\sigma_v = 1$). For NN interactions, one can write Eq. (34) as

$$\bar{\Gamma}_d(k) = k_d \sum_{j=0}^c n_j \exp(-\beta j J_{\text{NN}}), \quad (35)$$

where n_j denotes the number of occupied sites with j occupied NN sites, such that $\sum_{j=0}^c n_j = \eta_k$. Furthermore, by defining the probability $p_j = \langle n_j \rangle / \eta_k$ one has

$$\bar{\Gamma}_d(k) = k_d \eta_k \sum_j p_j \exp(-\beta j J_{\text{NN}}), \quad (36)$$

so that $\tilde{P}_k^f(\underline{x}) = p_j$ and the task is reduced to estimating $\sum_j p_j \exp(-\beta j J_{\text{NN}})$. This can easily be accomplished by evaluating the conditional probabilities $\{p_j\}_{j=0}^c$ of all occupied sites having j NN. This approach can easily be extended to longer-range interactions.

At constant pressure and temperature, $\{p_j\}_{j=0}^c$ is only a function of the coarse lattice coverage. There are two methods for computing p_j . One can generate *a priori* a database for $\{p_j\}_{j=0}^c$ using microscopic lattice KMC simulations for various values of coverage (see also Ref. 30 for use of this idea in boundary-value problems). However, this may be tedious for complex systems and will require interpolation and/or tabulation.

The second approach computes the equilibrium pdf $\{p_j\}_{j=0}^c$ within C_k at $\bar{\eta}_k$ on the fly using a microscopic lattice embedded within each coarse cell with $q_m \gg 1$ sites via, in our example, a canonical ensemble KMC simulation. The size of the microscopic lattice should be larger than the correlation length to avoid finite-size effects.² The microscopic lattice uses periodic boundary conditions and (η_m, q_m, T) as inputs. Its output is $p_j = \langle n_j \rangle / \eta_m$. Here $\eta_m = \text{int}(q_m \bar{\eta}_k)$ is the

number of particles on the microscopic lattice, where $\text{int}()$ is the greatest integer function. Details of the algorithm are mentioned in Sec. VI. Since there is always some uncertainty in the numerically ascertained $\{p_j\}_{j=0}^c$, the fact that η_m/q_m may not exactly match $\bar{\eta}_k$ does not affect the accuracy of the multigrid method as long as q_m is sufficiently large. $\langle n_j \rangle$ is obtained by time averaging n_j from a single trajectory calculation once the microscopic processes have reached local equilibrium.

Using the pdf $\{p_j\}_{j=0}^c$, the configurational energy of the cell is given by

$$\bar{H}_2(k) = -\frac{q}{2} \sum_{j=0}^4 j p_j J_{\text{NN}}. \quad (37)$$

As in the case of CGMC-QC, the coarse cell is assumed to be large ($q \rightarrow \infty$) and boundary effects are neglected. Thus, $\bar{H}_1(k) = 0$. The Hamiltonian is given by

$$\begin{aligned} \bar{H}(\underline{\eta}) &= \sum_{k \in \mathcal{L}_c} \bar{H}_2(k) + \sum_{k \in \mathcal{L}_c} \bar{h} \eta_k \\ &= -\frac{mq}{2} \sum_{j=0}^4 j p_j J_{\text{NN}} + \sum_{k \in \mathcal{L}_c} \bar{h} \eta_k. \end{aligned} \quad (38)$$

Since in the new method one solves the fast (slow) processes at small (large) length scales, hereafter, the method will be denoted as the multiscale CGMC method.

4. Connections to other literature methods

Multigrid methods have been applied in various contexts in the literature (see review in Ref. 10) mainly for deterministic, continuum partial differential equations (PDEs).³¹ In addition, multigrid MC methods have also been invoked to handle critical slow down when the sampling by MC becomes very inefficient due to the local updates of the lattice.^{32,33} Wavelets have also been applied successfully for coarse graining a fine-grid representation in both deterministic³⁴ and stochastic systems.³⁵ The overall idea of previous multigrid MC work is that one performs nonlocal (collective-mode) updating by solving a sequence of auxiliary problems on various grids of different size where random samples are generated from the Boltzmann distribution by heat-bath sweeps. These multigrid methods have a close root to block-spin renormalization-group theory and iterative multigrid methods used for PDEs and differ from the dynamic multiscale CGMC method presented here for arbitrary complex ensembles and processes. Our method has analogies to adaptive mesh refinement strategies for PDEs.^{36,37} The heterogeneous multiscale method and the related gap-tooth method^{38–40} couple usually different models (hybrid multiscale models) in different spatial domains and are conceptually closer to our approach.

In most available hybrid multiscale methods, information from the small length and time scales is computed via a microscopic molecular simulation, such as molecular dynamics, and passed often to deterministic conservation equations that evolve over large length and time scales. In turn, molecular simulations are carried out under an imposed external field determined from the macroscopic model. In such hybrid

multiscale models, lack of connection in the physics of models at different scales, i.e., in their corresponding constitutive equations, can result in the violation of conservation, numerical instabilities, and very importantly in incorrect noise passing between scales with unclear consequences for the physics of the problem studied.^{10,41} In contrast, the multiscale CGMC method is mathematically founded and does not exhibit numerical instabilities. In the limit of $q_m \rightarrow q$ and when no time scale separation is used, the method reduces to the conventional KMC. Furthermore, due to its nonhybrid nature and its probabilistic construction, it seamlessly preserves stochasticity at all scales, a feature currently impossible with any other available multiscale method, including wavelet transformations. Our method here builds upon our recent work on handling stiffness of reaction networks (singularly perturbed systems) in well-mixed environments²⁵ but extends it to spatially distributed systems by employing two grids and by capitalizing on our earlier mathematical work on the CGMC method.

V. DETAILED BALANCE

The reader is referred to Refs. 17 and 18, where it was shown that the CGMC-MF method obeys detailed balance. It is shown here that the CGMC-QC method also satisfies detailed balance. For example, in the case of exchange of particles between cell C_k and the fluid phase via adsorption and desorption, detailed balance requires that

$$\begin{aligned} \prod_{k \in \mathcal{L}_c} g_{\text{NN}} e^{-\beta \bar{H}} k_d P(q - \eta_k) \Big|_{\underline{\eta}} \\ = \prod_{k \in \mathcal{L}_c} g_{\text{NN}} e^{-\beta \bar{H}} k_d \sum_{v \in C_k} \langle \sigma_v e^{-\beta U_v} \rangle \Big|_{\underline{\eta} + \underline{\delta}_k}. \end{aligned} \quad (39)$$

Here $\underline{\delta}_k$ is a unit vector with the k th element being 1. Rearranging and retaining only the terms for cell C_k , one gets

$$\frac{g_{\text{NN}} e^{-\beta \bar{H}} \Big|_{\eta_k}}{g_{\text{NN}} e^{-\beta \bar{H}} \Big|_{\eta_{k+1}}} = \frac{k_d \sum_{v \in C_k} \langle \sigma_v e^{-\beta U_v} \rangle \Big|_{\eta_{k+1}}}{k_d P(q - \eta_k) \Big|_{\eta_k}}. \quad (40)$$

Using the maximum term method, one has

$$\frac{g_{\text{NN}} e^{-\beta \bar{H}} \Big|_{\eta_k}}{g_{\text{NN}} e^{-\beta \bar{H}} \Big|_{\eta_{k+1}}} = \frac{Q \Big|_{\eta_k}}{Q \Big|_{\eta_{k+1}}}. \quad (41)$$

Writing

$$Q \Big|_{\eta_{k+1}} = Q \Big|_{\eta_k} + \frac{dQ}{d\eta_k} \Big|_{\eta_k} + \dots \quad (42)$$

or

$$\frac{Q \Big|_{\eta_{k+1}}}{Q \Big|_{\eta_k}} = 1 + \frac{d \ln Q}{d\eta_k} \Big|_{\eta_k} + \dots = e^{-\beta \mu}. \quad (43)$$

Finally, using Eqs. (41) and (43) and $k_d P/k_d = Q_s$, one gets

TABLE III. Results from various stochastic closures used in computing $\sum_{v \in C_k} \langle \sigma_v e^{-\beta U_v} \rangle$ by various CGMC methods.

Closure/method	$\sum_{v \in C_k} \langle \sigma_v e^{-\beta U_v} \rangle$
Local mean-field theory	$\eta_k e^{-\beta \bar{U}_k}, \bar{U}_k = \bar{J}_{kk}(\eta_k - 1) + \sum_{l \in \mathcal{L}_c, l=k} \bar{J}_{kl} \eta_l$
Local quasichemical theory	$\begin{aligned} &0, & \bar{\eta}_k = 0 \\ &\eta_k \left[\frac{(\zeta_{\text{NN}} - 1 + 2\bar{\eta}_k)(1 - \bar{\eta}_k)}{(\zeta_{\text{NN}} + 1 - 2\bar{\eta}_k)\bar{\eta}_k} \right]^{c/2} e^{-\beta J_{\text{NN}}^{c/2}}, & 0 < \bar{\eta}_k < 1 \\ &e^{-\beta J_{\text{NN}}^c}, & \bar{\eta}_k = 1 \end{aligned}$
Multiscale, computational method	$\sum_x \sum_{v \in C_{k'}} \tilde{P}_{k'}(x) \sigma_v e^{-\beta U_v(x)}$

$$\langle \sigma_v e^{-\beta U_v} \rangle = \lambda Q_s (1 - \bar{\eta}_k). \quad (44)$$

According to Eqs. (22) and (26), both sides of Eq. (44) are equal. Thus detailed balance is satisfied.

For the multiscale CGMC scheme, the microscopic model on the fine lattice uses the KMC subject to the constraints of a coarse cell (in our example simply a canonical ensemble at a specified coverage) and it automatically satisfies detailed balance by suitable choice of the transition probabilities (Table I). Since equilibrium is unique and thus independent of the kinetics/transport processes involved, the transition probabilities of the slow processes, computed using microscopic local equilibrium configurations from the fine scale model of the fast processes, also obey detailed balance because they are simply ensemble averages of properly equilibrated microscopic states.

VI. ALGORITHM FOR CGMC-QC AND MULTISCALE CGMC METHODS

A. Implementation of the CGMC-QC method

The CGMC-QC method employs the conventional microscopic KMC algorithm, known also as stochastic simulation algorithm⁴² (SSA) but on a coarse grid with coarse transition probabilities (Tables II and III). It works similar to the CGMC-MF method and consists of the following steps:

- (1) Initialize the coarse lattice, the time ($t=0$), and the rate constants.
- (2) Compute the coarse-grained transition probabilities per unit time for all slow processes on the coarse lattice.
- (3) Select the $(K+1)$ th slow process randomly from all possible processes based on the criterion

$$\sum_{i=1}^K \bar{\Gamma}_i^s < \xi_{\text{tot}}^s \leq \sum_{i=1}^{K+1} \bar{\Gamma}_i^s, \quad (45)$$

where $\bar{\Gamma}_i^s$ is the transition probabilities per unit time of the i th slow process, $\bar{\Gamma}_{\text{tot}}^s$ is the sum of transition probabilities per unit time of all slow processes over the entire lattice, and ξ is a uniform random number $\in (0, 1)$.

- (4) Increment the time t by a continuous amount

$$\Delta t = -\ln \xi' / \bar{\Gamma}_{\text{tot}}^s, \quad (46)$$

where ξ' is the second random number from a uniform distribution.

- (5) Execute the $(K+1)$ th process by updating the coarse-grained occupancies.
- (6) If desirable time is reached, stop. Otherwise, return to step (2).

The slow processes involve adsorption and desorption with coarse transition probabilities per unit time given by Eqs. (7) and (27) (Tables II and III). Because of the similarities of the CGMC-MF and CGMC-QC methods, their computational requirements are nearly the same.

B. Implementation of the multiscale CGMC method

1. Accelerated time advancement and sampling on the coarse grid

The multigrid method is obviously computationally more expensive than the other analytical stochastic closures because of the microscopic lattice KMC simulations. However, further acceleration can result by realizing that when adsorbing or desorbing a particle no substantial change of the microscopic pdf occurs. This is true when the populations do not change substantially between events. Consequently, in this paper the pdf is kept fixed in time intervals during which

several adsorption and desorption events occur. Sampling on the coarse grid and calculation of time increments can follow the conventional KMC algorithm of one at a time process selection. However, the presence of coarse cells naturally allows one to fire bundles of slow processes at each time increment over the entire lattice instead of one at a time selection of KMC. Specifically, the binomial τ -leap method introduced in Ref. 14 for well-mixed systems and extended to the CGMC method (spatially distributed systems) in Ref. 43 is employed to select the time interval based on the r criterion⁴³

$$\tau = r \min_k (\eta_k / \bar{\Gamma}_d(k), (q - \eta_k) / \bar{\Gamma}_a(k)). \quad (47)$$

In well-mixed systems, Eq. is formally derived from a version of the ensemble-averaged difference-differential equation for each species by requiring that the change in the number of molecules per time step is sufficiently small. This equation has a form similar to the algebraic equations obtained by applying the explicit (first-order) Euler scheme to deterministic systems. The maximum value of the parameter r (and thus the maximum time step τ) is dictated from the absolute stability analysis of the difference-differential equation.⁴³ The adsorption $X_a(k)$ and desorption $X_d(k)$ bundles at C_k are sampled from a binomial distribution. Once the bundle size for all adsorption and desorption processes is determined, the coarse lattice is updated according to

$$\eta_k(t + \tau) = \eta_k(t) + X_a(k) - X_d(k), \quad k = 1, 2, \dots, m, \quad (48)$$

and the time is incremented by τ .

2. Initialization of the fine grid at each coarse time step

The estimation of the equilibrium pdf $\{p_j\}_{j=0}^c$ has to be computed for various coverages, and thus, proper initialization of the microscopic lattice can save some time to minimize the time needed to reach equilibrium within a coarse cell. The simpler approach is to store the final equilibrated microscopic configuration in each cell from the previous coarse time step, and use it at the new time step, while appropriately adding/removing particles from vacant/occupied sites according to the coarse-grid constraints. The reduction in CPU using this approach versus randomly placing particles on an initially empty microscopic lattice and then equilibrating the system is discussed in Sec. VII A. Alternatively, one may randomly place clusters based on the pdf from the last equilibration step so that η_m particles are present on the microscopic lattice.

3. Algorithmic details

A schematic of the multiscale CGMC algorithm is shown in Fig. 2. We execute the fast processes (diffusion) on the fine grid over short times using the KMC method and fire the slow coarse-grained (adsorption and desorption) processes over coarse, long time scales via the binomial τ -leap method. The algorithm can be outlined as follows:

- (1) Initialize the coarse lattice coverage $\{\bar{\eta}_k\}_{k=1}^m$, the time ($t=0$), the rate constants, and the numerical parameters

[the value of r for the binomial τ -leap method and the tolerance for testing the local equilibrium criterion, see step (5)]. Set the microscopic occupancy to zero and the net change in coarse lattice coverage $\Delta \bar{\eta}_k = \bar{\eta}_k$.

Fast scale/fine-grid KMC equilibration (microscopic integrator).

- (2) In each cell, if $\Delta \bar{\eta}_k > (<) 0$, randomly add (remove) $q_m |\Delta \bar{\eta}_k|$ particles to (from) vacant (occupied) microscopic lattice sites. Set the microscopic lattice time clock in each cell to $t_m = 0$.
- (3) For each coarse cell, partition a KMC simulation on a number of windows (intervals) of N_E MC events each. In each window, perform KMC on the microscopic lattice for the fast processes for N_E MC events. In each MC event:
 - (a) Select the $(K+1)$ th process from all possible fast processes based on the criterion $\sum_{i=1}^K \bar{\Gamma}_i^f < \xi \bar{\Gamma}_{\text{tot}}^f \leq \sum_{i=1}^{K+1} \bar{\Gamma}_i^f$, where the superscript f denotes fast process. Here $\bar{\Gamma}_{\text{tot}}^f$ is the sum of transition probabilities per unit time of all fast processes over the entire lattice.
 - (b) Increment the microscopic time t_m by $\Delta t_m^n = -\ln \xi' / \bar{\Gamma}_{\text{tot}}^f$.
 - (c) Execute the $(K+1)$ th fast process and update the microscopic lattice occupancies and transition probabilities per unit time.
- (4) Obtain the probability distribution function $\tilde{P}^f(\underline{x})$ for fast processes.
- (5) Test for local equilibrium condition.
 - (a) If the $\tilde{P}^f(\underline{x})$ obtained is from the first window of the microscopic integrator, then store the current pdf as $\tilde{P}^{f,\text{old}}(\underline{x}) = \tilde{P}^f(\underline{x})$ and go to step (3)(a).
 - (b) Otherwise, compare the current pdf $\tilde{P}^f(\underline{x})$ with the $\tilde{P}^{f,\text{old}}(\underline{x})$ and test for statistical convergence using the χ^2 method. If the two pdfs are the same (say with a probability of 99%) go to step (6) (after simulations in all coarse cells have been run). Otherwise, store the current pdf as $\tilde{P}^{f,\text{old}}(\underline{x}) = \tilde{P}^f(\underline{x})$ and go to step (3)(a).

Slow scale/coarse-grid binomial τ -leap CGMC.

- (6) Calculate the transition probabilities per unit time of all slow processes on the coarse lattice $\tilde{P}^f(\underline{x})$ [for example, see Eq. (36)] for all coarse cells.
- (7) Set $\bar{\eta}_{c,\text{old}} = \bar{\eta}_k$, $k = 1, \dots, m$.
- (8) Select a time leap τ based on the r criterion [Eq. (47)] and increment the coarse (macroscopic) time scale t by τ : $t = t + \tau$.
- (9) Compute the number of firings for each slow process using the binomial distribution.¹⁴
- (10) Update the populations of species of the coarse lattice based on Eq. (48) and the lattice coverage $\{\bar{\eta}_k\}_{k=1}^m$.
- (11) If desirable time is reached, stop. Otherwise, compute $\Delta \bar{\eta}_k = \bar{\eta}_k - \bar{\eta}_{k,\text{old}}$, $k = 1, \dots, m$ and return to step (2).

In order to obtain p_j during a KMC simulation of step (4), we compute the time-averaged number of sites n_j with j occupied NN sites, i.e., $\sum_{i=1}^{N_E} n_j \Delta t_m^i / t_m$ for $j=0, 1, \dots, c$. The probability distribution function p_j is given by $\sum_{i=1}^{N_E} n_j \Delta t_m^i / q_m t_m$, where t_m is the total time elapsed in the microscopic integrator.

VII. NUMERICAL ASSESSMENT OF THE CGMC-QC AND MULTISCALE CGMC METHODS

In this section, numerical simulations are carried out for a simple prototype system. Results from simulations of simultaneous adsorption, desorption, and diffusion on a periodic 2D lattice are reported.

A. Simulations in a uniform pressure field at high temperatures

The accuracy of the transient and equilibrium solutions of the KMC, CGMC-MF, CGMC-QC, and multiscale CGMC methods is first assessed. A spatially uniform external field (of pressure) is imposed. A total of $N=100 \times 100 = 10\,000$ sites are present on the KMC, CGMC-MF, and CGMC-QC lattices. Square coarse cells of size $q=10 \times 10 = 100$ are employed for the CGMC-MF and CGMC-QC simulations. The judiciously chosen small values of q and N allow comparisons of the CGMC methods with the computationally expensive KMC method on a single microscopic lattice. For the multiscale CGMC simulations, coarse cells of size $q=100 \times 100$ are employed, and the lattice contains $N=1000 \times 1000 = 1\,000\,000$ microscopic sites. The 2D microscopic lattice for multiscale CGMC contains $q_m=40 \times 40$ lattice sites (note that q_m is large but not much smaller than q . This choice is in order to have comparable results to the KMC method rather than to obtain high computational efficiency). To allow comparison of results of different CGMC methods, one coarse cell of the multiscale CGMC coarse lattice is compared to the entire lattice of KMC, CGMC-MF, and CGMC-QC methods. In actual applications, orders-of-magnitude larger q and N could be used in the CGMC methods. Such an example is presented in Sec. VII C. The multiscale CGMC simulations use a value of $r=0.1$ [in the r criterion, Eq. (47)] for the binomial τ -leap method. The separation of time scales in the physical process is chosen to be only about two orders of magnitude. While this is large enough to make the accuracy of the multiscale CGMC good, it is not representative of the much large stiffness encountered in physical systems, but KMC becomes prohibitive to use for stiffer systems than the one chosen here (see Sec. VII C for a much larger separation of time scales). The transient behavior is studied based on a single trajectory. Time-averaged equilibrium properties are obtained from a single trajectory over a long time window.

Figure 3 shows the average lattice coverage and the Hamiltonian versus time for the parameter values indicated in the figure. Five KMC trajectories with the same initial conditions but different seeds of the random generator are plotted as gray lines to aid visual comparison with CGMC methods in the presence of thermal fluctuations. A single trajectory is plotted for the CGMC-MF (dotted line), the

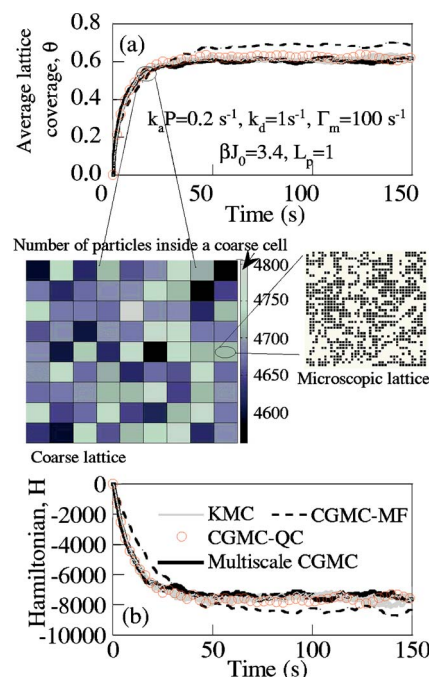


FIG. 3. (Color online) Comparison of the (a) time-dependent average lattice coverage and the (b) Hamiltonian of various methods. Parameters are mentioned in the figure. Snapshots of the coarse lattice ($m=10 \times 10$ coarse cells) and the microscopic lattice ($q_m=40 \times 40$ lattice sites) from the multiscale CGMC simulation at time $t=10$ s are shown.

CGMC-QC (circles), and the multiscale CGMC (dark line) methods. Strong NN attractive intermolecular interactions result in a significant error in both transient and equilibrium solutions of the CGMC-MF method. On the other hand, both the CGMC-QC and multiscale CGMC methods are in good agreement with the KMC results.

A snapshot of the coarse lattice of the multiscale CGMC method at time $t=10$ s is also shown. Each coarse cell has a different number of particles, as shown by the shaded bar depicting the effect of fluctuations at the coarse-grid scale. A snapshot of the microscopic lattice embedded in one coarse cell of the multiscale method is also shown in Fig. 3. Inhomogeneity in the distribution of particles on the fine grid underscores the effect of spatial correlations caused by intermolecular forces within a coarse cell. Only the multiscale CGMC retains that correct spatial distribution of particles inside a coarse cell.

As mentioned earlier the microscopic lattice can be initialized in different ways before equilibrium statistics is obtained. Figure 4 shows the evolution of the Hamiltonian of the microscopic lattice during the equilibration process starting from two different initial configurations at $t=10$ s. In the first initialization approach, $\eta_m = \text{int}(q_m \bar{\eta}_k)$ particles are randomly placed on an empty microscopic lattice at $t_m=0$. The second approach follows Sec. VI B, wherein particles are added/removed from the last equilibrium configuration of the microscopic lattice. Note that both approaches yield the same pdf. However, as evident from Fig. 4 the second method requires fewer MC events and is thus more economical. In fact, by using a microscopic state from the previous macroscopic time step, the system is already close to equilibrium despite τ leaping. Thus, it may be possible to maintain the

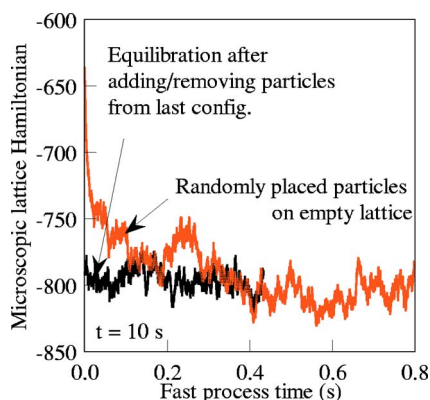


FIG. 4. (Color online) Hamiltonian on the fine grid vs time toward equilibrium by fast diffusion at macroscopic time $t=10$ s for two initializations (see text) of the microscopic lattice in the multiscale CGMC simulation of Fig. 3. Random placement of particles needs some time for equilibration. Using a microscopic configuration from the previous macroscopic time step results in faster relaxation.

same pdf even for more than one τ leap, resulting in further time acceleration. On the other hand, an initial random distribution of particles forms clusters (relaxes) over a longer period of time. It is important to note that the time scale for equilibration is much shorter than that of the coarse time scale shown in Fig. 3. This is a direct result of the separation of time scales between fast and slow processes and highlights the time acceleration of the multiscale CGMC method (albeit relatively moderate for our choice of parameters).

Figure 5 shows the total number of particles adsorbing and desorbing on the coarse lattice per time leap for the multiscale simulation depicted in Fig. 3. As shown in Fig. 5, initially no desorption events occur on the empty lattice, whereas at equilibrium the adsorption and desorption bundle sizes match. Unlike the one process per time step of a KMC algorithm, the binomial τ -leap method allows several processes to simultaneously occur over the entire lattice in a single but larger time leap. This τ -leaping feature makes the multiscale method more economical. We have shown before both theoretically and via simulation that the binomial τ -leap method becomes very advantageous as the cell size and the lattice size increase.⁴³

While comparison of single trajectories shown in Fig. 3 is a good starting point, pdfs of various quantities provide a

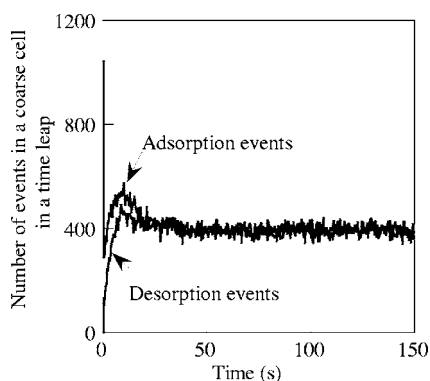


FIG. 5. Number of adsorption and desorption events (i.e., the bundle size) in a single time leap in a coarse cell with the binomial τ -leap multiscale CGMC method vs time for the simulation depicted in Fig. 3.

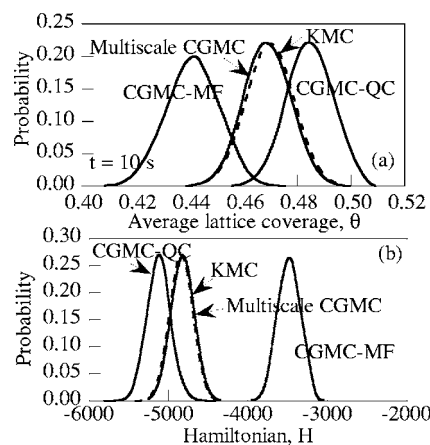


FIG. 6. Probability distribution function for (a) the average lattice coverage θ and (b) the Hamiltonian at time $t=10$ s from different methods for the simulation depicted in Fig. 3. The KMC and multiscale CGMC method pdfs are statistically indistinguishable.

more strict comparison of stochastic methods. Using averaging over 1000 trajectories with the conditions of Fig. 3, we have determined the pdfs of the coverage and of the Hamiltonian of the various methods. These pdfs are compared in Fig. 6. The presence of spatial correlations makes comparison of the Hamiltonians of different methods a more strict measure compared to coverages. The CGMC-MF method underpredicts the average lattice coverage and the Hamiltonian, whereas the CGMC-QC method over- (under-) predicts the coverage (Hamiltonian). The deviation from the correct average lattice coverage is nearly the same for the two methods. On the other hand, the KMC and multiscale CGMC pdfs are statistically indistinguishable.

The error of various methods with respect to the exact KMC as a function of the equilibrium average lattice coverage θ is plotted in Fig. 7. θ is varied by changing $k_a P/K_d$. Other parameters are the same as in Fig. 3. The error in the CGMC-MF solution can be up to eight times larger than the corresponding one of the CGMC-QC method. The error of the multiscale CGMC method is statistically insignificant.

When small length scale features, such as boundaries, interfaces, and sharp gradients,^{44,45} are present and demand microscopic resolution, CGMC can become computationally demanding. In such cases, adaptive (nonuniform lattices) CGMC simulations^{26,46} should be used. Extension of the CGMC-QC and multiscale CGMC methods to nonuniform lattices is straightforward but these techniques should be applied only in large coarse cells beyond a certain cutoff cell size. For example, Fig. 8 shows the error in CGMC-MF and CGMC-QC equilibrium coverages as a function of the coarse-cell size q . The CGMC-MF and CGMC-QC errors show opposite trends. The CGMC-MF (CGMC-QC) error increases (decreases) with increasing cell size q . There is a crossover point at $q=40$ above which the CGMC-QC method is more accurate than the CGMC-MF method. By construction, the CGMC-MF method reduces to the KMC when $q=1$ and approaches the global MF theory when $q \rightarrow \infty$. As a result, the error in the CGMC-MF method approaches an asymptotic limit as the coarse-cell size varies. On the other hand, information loss theory indicates that the

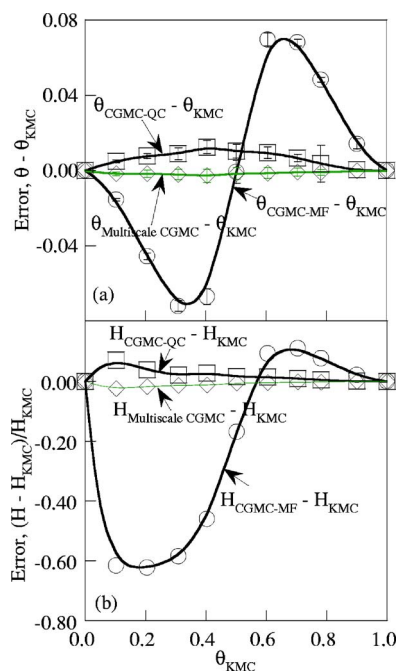


FIG. 7. (Color online) Error in (a) the average lattice coverage and (b) the Hamiltonian of different CGMC methods in comparison to the KMC method. The error reduces in the following order: CGMC-MF, CGMC-QC, and multiscale CGMC methods. The adsorption prefactor $k_a P$ is varied to achieve different average lattice coverages, θ .

error in CGMC-MF scales as $O(q/L_p)^{18,27}$. For short-ranged interactions, such as $L_p=1$, this error is “large” even when $q=2$. Since the method is exact at $q=1$ and q is an integer number, a discontinuous (abrupt) increase in the error occurs, as shown in Fig. 8 (here results are depicted for q starting at 4). The large errors in the CGMC-QC method for small values of q result from the QC approximation being valid for $q \rightarrow \infty$. In fact, when q is small, one hardly has enough pairs for the bulk statistical-mechanics equations to hold. It appears that the MF closure of random distribution of particles is a better approximation than the QC one when coarse cells are small in size.

B. Simulations in a uniform pressure field at low temperatures

The above simulations are carried out when the isotherm is single valued, i.e., at sufficiently high temperatures. Figure

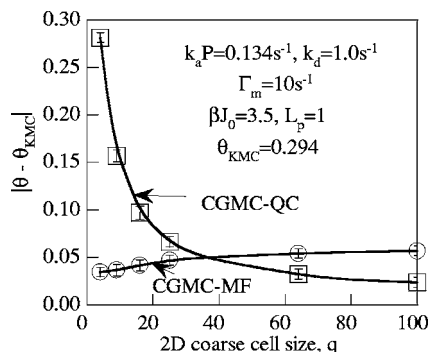


FIG. 8. Error in the average equilibrium lattice coverage θ of the CGMC-MF and CGMC-QC from the KMC method as a function of the cell size q for the parameters indicated. For these parameters KMC gives an average lattice coverage of $\theta_{KMC}=0.294$. The error in the CGMC-QC becomes smaller than that of the CGMC-MF method after roughly $q=40$.

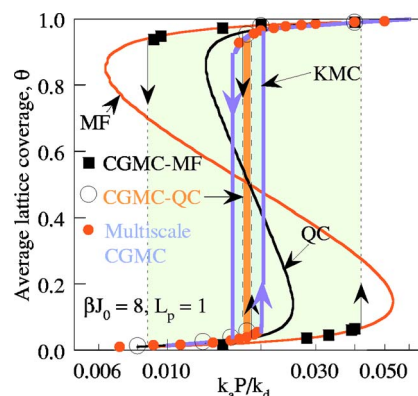


FIG. 9. (Color online) Adsorption isotherms of various methods for low temperatures ($\beta J_0=8$). The adsorption isotherms using the global QC theory [Eq. (22)] and the global MF theory are denoted as QC and MF, respectively (wider multiplicity regimes). Excellent agreement is observed between the multiscale CGMC and KMC simulations.

9 shows the adsorption isotherms of various methods for a temperature ($\beta J_0=8$) that is lower than the critical temperature. Under these conditions multiplicity in the adsorption isotherm occurs. In this case it is important that the coarse KMC simulator samples from the appropriate pdf of the corresponding microscopic states so the correct branch of the isotherm is obtained. More importantly, calculation from an average state could lead to a single-valued, nonhysteretic isotherm especially if the microscopic lattice is too small to allow multiple transitions between the two branches.

The global MF approximation results in the widest multiplicity regime with the global QC theory [Eq. (22)] giving results closer to those of the KMC method (a well-known fact). Due to thermal fluctuations, the CGMC-QC isotherm (open circles) has a smaller multiplicity regime than that of the KMC method. In contrast, the multiscale CGMC method gives results similar to the KMC method (within statistical difference).

C. Simulations in a nonuniform pressure field

Finally, numerical simulations are carried out for a $0.5\text{-mm} \times 5\text{-}\mu\text{m}$ -sized lattice containing 10^{10} microscopic lattice sites (with a lattice constant of 5 \AA) to assess the computational requirements of the various CGMC methods. These calculations are carried out in a nonuniform pressure field, a situation that is more realistic of physical systems. Specifically, the adsorption prefactor $k_a P$ varies linearly, as shown in Fig. 10(b), along the long dimension of the lattice (denoted as x axis) and is uniform along the perpendicular y axis. The other parameters are $k_d=1\text{ s}^{-1}$, $\Gamma_m=10^5\text{ s}^{-1}$, and $\beta J_0=3.5$. The resulting time scale separation of $O(10^5)$ is comparable to the stiffness encountered in realistic systems. The coarse lattice contains 100 initially empty coarse cells and each coarse cell consists of $10^4 \times 10^4$ microscopic sites. Simulations were performed on a single 1.8 GHz Pentium Xeon processor.

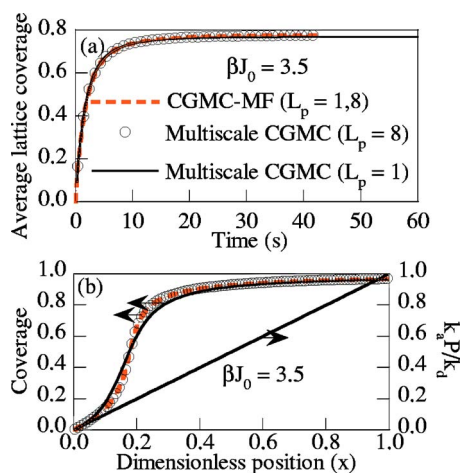


FIG. 10. (Color online) Transient, average lattice coverage and (b) steady-state coverage in the presence of adsorption and desorption and 10^5 times faster diffusion on a $0.5 \text{ mm} \times 5 \mu\text{m}$ lattice with 10^{10} microscopic sites. A nonuniform adsorption prefactor [$k_a P$ shown in (b)] results in a nonuniform coverage along the lattice. Only the multiscale CGMC method can resolve the correct coverage profile for short potentials.

The lattice uptake and the steady-state coverage profile are plotted in Figs. 10(a) and 10(b), respectively, for various methods. After 3 h of CPU the CGMC-MF simulations captured only 0.12 s of real time, and this method was not further pursued. Longer time scales were accessed only by simultaneously coarse graining space and time. The CGMC-MF method combined with the binomial τ -leap method⁴³ captured 40 s real time in a 20-s-long simulation (dashed line in Fig. 10). The multiscale method is computationally more expensive than the CGMC-MF method, due to the microscopic KMC simulator, and required 5–8 h for $L_p=1$ and 8 for capturing 40 s of real time. Note that the corresponding KMC simulation is estimated to take $q=10^8$ times longer, i.e., 34 000 years long.

The CGMC-MF method gives identical results for both short- ($L_p=1$) and longer- ($L_p=8$) ranged interactions given that the coarse-grained cell is much larger than L_p , so effectively the range of the potential plays no role (mean-field behavior is established with negligible cell-cell interactions). As mentioned earlier the CGMC solution matches asymptotically with MF results in the limit of infinitely long-ranged interactions. This practically happens for relatively medium-range potentials when the dimensionality of the system is high (here 2D). Consequently, both the multiscale CGMC (open circles) and CGMC-MF solutions are in good agreement when $L_p=8$. On the other hand when $L_p=1$, only the multiscale CGMC method (solid line) gives the correct solution [this is more easily discerned in the steady-state profile of Fig. 10(b)]. The differences in accuracy are not that dramatic for this relatively high temperature.

The microscopic lattice inside each coarse cell in the multiscale CGMC method simulations contains 40×40 microscopic sites. Length and time scales of the order of 10 nm and 10 μs were accessed on the microscopic lattice, whereas the corresponding scales on the coarse lattice are 0.1 mm and 100 s (see Fig. 11).

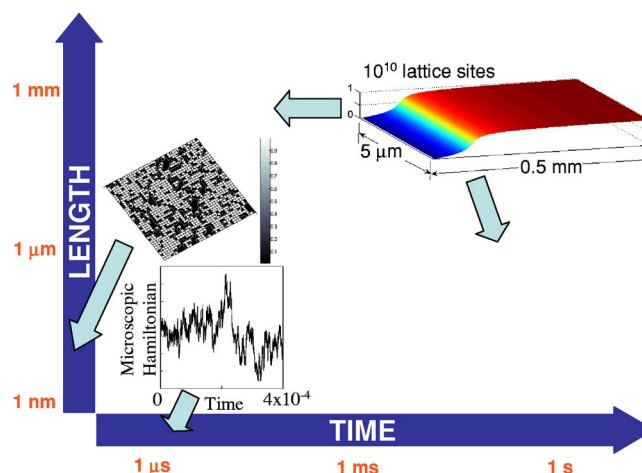


FIG. 11. (Color online) Length and time scales accessed by the microscopic and coarse lattices of the multiscale CGMC simulations of Fig. 10. The microscopic simulator operates over short length and time scales (of the order of 10 nm and 10 μs) to obtain the cluster pdfs. These pdfs are used in coarse simulations to reach length and time scales of the order of 0.1 mm and 100 s.

VIII. CONCLUSIONS

In this paper, the previously introduced coarse-grained Monte Carlo (CGMC) method, which was based on a local mean-field (MF) stochastic closure, for performing spatial MC simulation was revised. The CGMC methods provide a general nonequilibrium statistical-mechanics framework to coarse grain space and time in a discrete probabilistic KMC model. The method is applicable when two conditions are satisfied. First, there should be a clear-cut time scale separation, so that fast processes attain local equilibrium over very short time scales in comparison to the slow processes. Second, the simulated domain should be very large, so that significant spatial coarse graining is possible.

Given large time scale separation, it was proposed that a hierarchy of stochastic closures can be employed to account for higher moments of the cluster probability distribution function (pdf) and improve the accuracy of the CGMC method while obeying detailed balance. One approach enforces stochastic closure by employing analytical expressions of higher-order approximations of the cluster pdf. A derivation was presented for one such approximation, namely, the quasichemical (QC) approximation, and it was numerically shown that the resulting CGMC-QC method is more accurate than the CGMC-MF method for first nearest-neighbor (NN) interactions. The time requirements with the CGMC-MF and CGMC-QC methods are nearly the same. However, the QC approximation is applicable only to isotropic potentials with NN interactions. Furthermore, at low temperatures, strong interactions, and short-ranged potentials, a large number of moments of the underlying pdf is needed. This is a daunting task for multicomponent systems with complex chemistry. In order to overcome these obstacles, a second computationally based approach, namely, the multiscale CGMC method, was introduced. The multiscale CGMC method operates at two lengths and two time scales (extension to more scales is straightforward), similar to having two coupled integrators, one for the stiff problem and

one for the nonstiff problem. A coarse grid is used to advance the slow processes over long time scales with time increments that account for firing of multiple processes over the entire lattice (τ leaping). This consists the macroscopic integrator. A microscopic KMC simulation is carried out on a small, fine-grid lattice embedded within each coarse cell for short periods of time. This fine-grid/short time scale KMC consists the microscopic integrator. It estimates numerically the cluster pdf and coarse transition probabilities of the coarse integrator. In turn the coarse integrator provides the coarse variables under which the microscopic KMC must be conducted at each coarse cell. The mathematical underpinnings of the method for correctly coupling scales were given. Results from the exact microscopic KMC and multiscale CGMC simulations have been found to be statistically indistinguishable. Its multigrid nature renders the multiscale CGMC method reminiscent of a microscope with variable resolution (see Fig. 3).

The multiscale CGMC method is generic and provides accuracy but at increased computational cost compared to the analytically based CGMC methods. Currently, it is the only spatial coarse-grained Monte Carlo method that provides accuracy and efficiency, no numerical instabilities, and ensures correct noise passing between scales. The method has been employed successfully in well-mixed systems containing multiple molecular species and reaction processes in Ref. 25, capitalizing on time scale separation only. Extension of CGMC to complex systems, including multicomponent species, an arbitrary lattice with multiple types of lattice sites, and many molecular processes, is entirely possible. Possible applications of multiscale CGMC methods include catalysis, epitaxial growth, diffusion in microporous membranes, atmospheric science, and biology. Future work will focus on such applications of complex systems.

ACKNOWLEDGMENT

The research was partially supported by the NSF through CTS-0312117.

APPENDIX: SINGULAR PERTURBATION ANALYSIS FOR THE LATTICE MODEL

One starts with the difference-differential equation [Eq. (6)]

$$d\sigma_v = \Gamma_a(v)dt - \Gamma_d(v)dt + \sum_{v' \in B_v} (\Gamma_{\text{mig}}(v' \rightarrow v)dt - \Gamma_{\text{mig}}(v \rightarrow v')dt), \quad v \in C_k, \quad (\text{A1})$$

where B_v is the set of sites around v to (from) which diffusion from (to) site v can occur. For example, B_v may contain the first NN sites. Adding the ensemble-averaged transition probabilities per unit time on all sites in a coarse cell C_k

one gets

$$d \sum_{v \in C_k} \langle \sigma_v \rangle = dt \sum_{v \in C_k} \left\{ k_a P (1 - \langle \sigma_v \rangle) - k_d \langle \sigma_v e^{-\beta U_v} \rangle + \frac{\Gamma_m}{4} \sum_{v' \in B_v} (\langle \sigma_{v'} (1 - \sigma_v) e^{-\beta U_v} \rangle - \langle \sigma_v (1 - \sigma_{v'}) e^{-\beta U_v} \rangle) \right\}. \quad (\text{A2})$$

Let $\max(k_a P, k_d)/\Gamma_m = \varepsilon \ll 1$. For illustration we take $k_d/k_a P = \omega \sim 1$ and set $k_a P/\Gamma_m = \varepsilon$. We first focus on the short time scales. Introducing the dimensionless fast time scale $\tilde{t}_f = \Gamma_m t$, Eq. (A2) becomes

$$d \sum_{v \in C_k} \langle \sigma_v \rangle = d\tilde{t}_f \sum_{v \in C_k} \left\{ \varepsilon (1 - \langle \sigma_v \rangle) - \varepsilon \omega \langle \sigma_v e^{-\beta U_v} \rangle + \frac{1}{4} \sum_{v' \in B_v} (\langle \sigma_{v'} (1 - \sigma_v) e^{-\beta U_v} \rangle - \langle \sigma_v (1 - \sigma_{v'}) e^{-\beta U_v} \rangle) \right\} \quad (\text{A3})$$

that gives us $\varepsilon \rightarrow 0$

$$d \sum_{v \in C_k} \langle \sigma_v(\tilde{t}_f) \rangle = \frac{1}{4} d\tilde{t}_f \sum_{v \in C_k} \sum_{v' \in B_v} (\langle \sigma_{v'} (1 - \sigma_v) e^{-\beta U_{vv'}} \rangle - \langle \sigma_v (1 - \sigma_{v'}) e^{-\beta U_{vv'}} \rangle). \quad (\text{A4})$$

The configuration space at short time scales evolves due to fast processes (in our case diffusion) according to Eq. (A4). During short time scales, the slow variables remain fixed but the values of slow variables constrain the dynamics of fast processes. More explicitly, diffusion within a coarse cell occurs at a specified coverage provided by the slow processes of adsorption and desorption.

Next, introducing the dimensionless slow time scale $\tilde{t}_s = k_a P t$, Eq. (A2) becomes

$$d \sum_{v \in C_k} \langle \sigma_v \rangle = d\tilde{t}_s \sum_{v \in C_k} \left\{ (1 - \langle \sigma_v \rangle) - \omega \langle \sigma_v e^{-\beta U_v} \rangle + \frac{1}{4\varepsilon} \sum_{v' \in B_v} (\langle \sigma_{v'} (1 - \sigma_v) e^{-\beta U_{vv'}} \rangle - \langle \sigma_v (1 - \sigma_{v'}) e^{-\beta U_{vv'}} \rangle) \right\}. \quad (\text{A5})$$

Since $\varepsilon^{-1} \gg 1$, from Eq. (A5) one gets

$$d \sum_{v \in C_k} \langle \sigma_v(\tilde{t}_s) \rangle = d\tilde{t}_s \sum_{v \in C_k} (1 - \langle \sigma_v \rangle) - \omega \langle \sigma_v e^{-\beta U_v} \rangle \quad (\text{A6})$$

subject to

$$\sum_{v \in C_k} \sum_{v' \in B_v} (\langle \sigma_{v'} (1 - \sigma_v) e^{-\beta U_{vv'}} \rangle - \langle \sigma_v (1 - \sigma_{v'}) e^{-\beta U_{vv'}} \rangle) = 0. \quad (\text{A7})$$

Equation (A6) is obtained when Eq. (A4) reaches local equilibrium. The configuration space at long time scales evolves due to the slow processes according to Eq. (A6) while satisfying Eq. (A6) due to the fast processes. In other words, the underlying pdf within a coarse cell is slaved to the slow variables.

- ¹G. H. Gilmer, H. C. Huang, T. D. de la Rubia, J. Dalla Torre, and F. Baumann, *Thin Solid Films* **365**, 189 (2000).
- ²*Monte Carlo Methods in Statistical Physics*, edited by K. Binder (Springer-Verlag, Berlin, 1986), Vol. 7.
- ³D. P. Landau and K. Binder, *A Guide to Monte Carlo Simulations in Statistical Physics* (Cambridge University Press, Cambridge, 2000).
- ⁴T. S. Shimizu, S. V. Aksenov, and D. Bray, *J. Mol. Biol.* **329**, 291 (2003).
- ⁵S. M. Auerbach, *Int. Rev. Phys. Chem.* **19**, 155 (2000).
- ⁶L. D. Shea, G. M. Omann, and J. J. Linderman, *Biophys. J.* **73**, 2949 (1997).
- ⁷B. Khouider, A. J. Majda, and M. Katsoulakis, *Proc. Natl. Acad. Sci. U.S.A.* **100**, 11941 (2003).
- ⁸H. Brune, *Surf. Sci. Rep.* **31**, 121 (1998).
- ⁹S. Raimondeau and D. G. Vlachos, *Chem. Eng. J.* **90**, 3 (2002).
- ¹⁰D. G. Vlachos, *Adv. Chem. Eng.* **30**, 1 (2005).
- ¹¹D. T. Gillespie, *J. Chem. Phys.* **115**, 1716 (2001).
- ¹²M. Rathinam, L. R. Petzold, Y. Cao, and D. T. Gillespie, *J. Chem. Phys.* **119**, 12784 (2003).
- ¹³T. Tian and K. Burrage, *J. Chem. Phys.* **121**, 10356 (2004).
- ¹⁴A. Chatterjee, D. G. Vlachos, and M. Katsoulakis, *J. Chem. Phys.* **122**, 024112 (2005).
- ¹⁵H. Resat, H. S. Wiley, and D. A. Dixon, *J. Chem. Phys.* **105**, 11026 (2001).
- ¹⁶M. Katsoulakis, A. J. Majda, and D. G. Vlachos, *Proc. Natl. Acad. Sci. U.S.A.* **100**, 782 (2003).
- ¹⁷M. A. Katsoulakis and D. G. Vlachos, *J. Chem. Phys.* **119**, 9412 (2003).
- ¹⁸M. A. Katsoulakis, A. J. Majda, and D. G. Vlachos, *J. Comput. Phys.* **186**, 250 (2003).
- ¹⁹T. L. Hill, *An Introduction to Statistical Thermodynamics* (Dover, New York, 1986).
- ²⁰C. W. Gardiner, *Handbook of Stochastic Methods*, 2nd ed. (Springer-Verlag, Berlin, 1985).
- ²¹R. Ghez, *A Primer of Diffusion Problems* (Wiley, New York, 1988).
- ²²D. G. Vlachos and M. A. Katsoulakis, *Phys. Rev. Lett.* **85**, 3898 (2000).
- ²³R. Lam, T. Basak, D. G. Vlachos, and M. A. Katsoulakis, *J. Chem. Phys.* **115**, 11278 (2001).
- ²⁴C. V. Rao and A. P. Arkin, *J. Chem. Phys.* **118**, 4999 (2003).
- ²⁵A. Samant and D. G. Vlachos, *J. Chem. Phys.* **123**, 144114 (2005).
- ²⁶A. Chatterjee, D. G. Vlachos, and M. A. Katsoulakis, *J. Chem. Phys.* **121**, 11420 (2004).
- ²⁷A. Chatterjee, D. G. Vlachos, and M. Katsoulakis, *Int. J. Multiscale Comp. Eng.* **3**, 59 (2005).
- ²⁸T. L. Hill, *Statistical Mechanics: Principles and Selected Applications* (Dover, New York, 1987).
- ²⁹J. S. Reese, S. Raimondeau, and D. G. Vlachos, *J. Comput. Phys.* **173**, 302 (2001).
- ³⁰D. G. Vlachos, *AIChE J.* **43**, 3031 (1997).
- ³¹W. L. Briggs, V. E. Henson, and S. F. McCormick, *A Multigrid Tutorial*, 2nd ed. (SIAM, Philadelphia, PA, 2000).
- ³²J. Goodman and A. D. Sokal, *Phys. Rev. D* **40**, 2035 (1989).
- ³³D. Kandel, E. Domany, and A. Brandt, *Phys. Rev. B* **40**, 330 (1989).
- ³⁴A. R. Mehrabi and M. Sahimi, *Phys. Rev. Lett.* **79**, 4385 (1997).
- ³⁵A. E. Ismail, G. C. Rutledge, and G. Stephanopoulos, *J. Chem. Phys.* **118**, 4414 (2003).
- ³⁶M. Gummalla, M. Tsapatsis, J. J. Watkins, and D. G. Vlachos, *AIChE J.* **50**, 684 (2004).
- ³⁷M. J. Berger and J. Oliger, *J. Comput. Phys.* **53**, 484 (1984).
- ³⁸E. Weinan, B. Engquist, and Z. Y. Huang, *Phys. Rev. B* **67**, 092101 (2003).
- ³⁹C. W. Gear, J. Li, and I. G. Kevrekidis, *Phys. Lett. A* **316**, 190 (2003).
- ⁴⁰J. W. Evans and M. S. Miesch, *Surf. Sci.* **245**, 401 (1991).
- ⁴¹T. P. Schulze, *J. Cryst. Growth* **263**, 605 (2004).
- ⁴²D. T. Gillespie, *J. Comput. Phys.* **22**, 403 (1976).
- ⁴³A. Chatterjee and D. G. Vlachos, *J. Comput. Phys.* **211**, 596 (2006).
- ⁴⁴G. Ertl, *Science* **254**, 1750 (1991).
- ⁴⁵W. K. Burton, N. Cabrera, and F. C. Frank, *Proc. R. Soc. London, Ser. A* **243**, 299 (1951).
- ⁴⁶A. Chatterjee, M. A. Katsoulakis, and D. G. Vlachos, *Phys. Rev. E* **71**, 026702 (2005).